On the causes of trends in the seasonal amplitude of atmospheric CO_2

The observed increase in the seasonal amplitude of atmospheric CO_2 in the northern latitudes reveals major ecological changes that are not captured by terrestrial ecosystem models participating in the fifth phase of the Coupled Model Intercomparison Project (CMIP5) (Graven et al., 2013). Here, we used atmospheric CO_2 records from 26 northern hemisphere stations with coverage longer than 15 years, and the LMDZ4 atmospheric transport model prescribed with Net Ecosystem CO_2 Exchange (NEE) from an ensemble of nine terrestrial ecosystem models, to attribute change in the seasonal amplitude of atmospheric CO_2. We found significant ($P<0.05$) increases in seasonal peak-to-trough CO_2 amplitude (AMP_{P-T}) at 9 stations, and in trough-to-peak amplitude (AMP_{T-P}) at 8 stations over the last three decades. Most of the stations with an increasing amplitude are located in Arctic and boreal regions (>50°N), consistent with previous observations that the amplitude increased faster at Barrow (Arctic) than at Mauna Loa (subtropics). The multi-model ensemble mean (MMEM) shows that the physiological response of ecosystems to rising CO_2 concentration (eCO_2) and climate change are dominant drivers of the increase in AMP_{P-T} and AMP_{T-P} in the high latitudes. At the Barrow station, the observed increase of AMP_{P-T} and AMP_{T-P} over the last 33 years is explained by eCO_2 (39% and 42%) almost equally than by climate change (32% and 35%). The increased carbon losses during carbon release period in response to eCO_2 are related to an enhancement of ecosystem respiration due to the eCO_2 caused increase in carbon storage during carbon uptake period. We also found smaller contributions of air-sea CO_2 fluxes (10% for AMP_{P-T} and 11% for AMP_{T-P}) and marginally significant impacts of change in land use (3% for AMP_{P-T} and 4% for AMP_{T-P}) at Barrow, highlighting the important role of these factors in regulating change in seasonal cycle of global carbon cycle, which has been generally ignored by previous studies.

Introduction

As an integrated signal of large scale ecological changes, the change in seasonal variations of atmospheric CO_2 concentration is an emerging property of the carbon cycle (e.g. Bacastow et al., 1985; Kohlmaier et al., 1989; Keeling et al., 1996; Randerson et al., 1997; Piao et al., 2008; Graven et al., 2013; Zeng et al., 2014; Gray et al., 2014; Barlow et al., 2015; Forkel *et al.*, 2016). The seasonal CO_2 amplitude (AMP) in the lower troposphere has increased by ≈ 50% north of 45°N since the 1960s (Graven et al., 2013), and this signal can only be explained by an increased seasonality of net biome productivity (NBP) in boreal and northern temperate ecosystems. Yet, there is no consensus on the major factors driving the increase of NBP and the quantitative contribution of other, smaller fluxes like fossil CO_2 emissions and air-sea exchange. On the one hand, Gray et al., (2014) and Zeng et al., (2014) suggested that agricultural improvements contributed to the increase of AMP by increasing the seasonal NBP uptake in cultivated lands, but there is a two-fold difference in the estimated contribution of this mechanismin in the two studies (range 17%-45% of the increasing AMP). On the other hand, Randerson et al. (1997) and Forkel et al. (2016) showed that during the last three decades, most of the increase of amplitude took place at stations north of 55°N. In this view, agriculture improvement seems unlikely to be the only driving factor, because croplands are mainly in northern temperate latitudes (Foley et al., 2005). Using the LPJmL carbon cycle model with an improved phenology module coupled with the TM3 atmospheric transport model, Forkel et al. (2016) found that it is mainly the physiological response of northern plants to warming rather to increasing CO_2 that explains the trend of AMP over the last 20 years, which is partly inconsistent with the observation made by Graven et al. (2013) that AMP increased in the 1960s to the mid-1970s at a time when northern temperature slightly decreased, highlighting the need to search deeper in the attribution of the AMP trend.

In this paper, we investigate the AMP trend in the northern hemisphere over the last thirty years (1980-2012) using an ensemble of ecosystem models with different parameterizations of the effect of elevated CO_2 and climate change (TRENDYv2) (Sitch et al., 2015) with another transport model (LMDZ4) (Hourdin et al., 2013). We also separate the contribution of fossil fuel CO_2 emissions, air-sea fluxes as well as the effect of climate change, rising CO_2 (eCO_2), nitrogen deposition in some models and land use change on the trends in the seasonality of land ecosystem exchange. The contribution of atmospheric transport trends to AMP trends is further analyzed. Trends in seasonal atmospheric CO_2 from 26 northern (north of 23°N) long-term atmospheric stations (>15 years in the period of 1980-2012) of the NOAA-ERSL surface flask air-sampling network (Table S1 and Figure S1) are used.

Results and Discussion

Observed CO_2 data

The 26 northern (north of 23°N) atmospheric stations selected are shown in Figure S1 and Table S1. According to the shape of detrended CO_2 seasonal cycle (Thoning et al., 1989, see methods) (Figure S2), we divided the amplitude into peak-to-trough (AMP_{P-T}, defined as the difference between the peak value and the trough value of CO_2 seasonal cycle in a year) and trough-to-peak (AMP_{T-P}, defined as the difference between the trough value of CO_2 seasonal cycle in a year and the peak value of the cycle in the next year). As shown in Figure 1a, a significant ($P<0.05$) positive trend of AMP_{P-T} ranging from 0.05 to 0.15 ppm yr^{-1} is found at 9 stations, 8 of them being north of 50°N. The other stations do not show significant positive AMP_{P-T} trends and 5 stations show negative trends (the latter being significant at only one station UUM). The significant increase in AMP_{P-T} reflects mainly an increasing CO_2 drawdown (defined by the monthly net CO_2 concentration change) in June and July (Figure S3).

The trends in AMP_{T-P} reported in Table S1 are similar to those of $AMP_{P-T,}$ logically expected because we remove a long-term mean trend of each CO_2 time series (Figure. 1b). In total, 7 out of 8 stations with a significant ($P<0.05$) increase of AMP_{T-P} during 1980-2012 are located north of 50°N. The months of September and October are those during which most of the negative trend of AMP_{T-P} occurs at those sites (Figure S3). Overall, no sties show significant positive trend in AMP_{T-P} during the study period.

Terrestrial ecosystem output and simulation of CO_2 amplitude trends

The Net Ecosystem CO_2 Exchange (NEE) from Eight dynamic global vegetation models (DGVMs) from TRENDYv2 (Le Quéré et al., 2014; Sitch et al., 2015) (Table S2) was prescribed to the atmospheric transport model (LMDZ4) (Hourdin et al., 2013, See Methods). Time-varying monthly NEE from each model under simulation S3 (driven by CO_2, climate change and land-cover change) (Sitch et al., 2015), fossil fuel and cement emissions (Andres et al., 2011; Boden et al., 2016), and interannual air-sea fluxes (Buitenhuis et al., 2010) were prescribed to the global LMDZ4 transport model (Hourdin et al., 2013) with variable winds over the last 33 years. This is the T1 simulation (see Methods and Table 4), from which the modeled CO_2 concentration field was sampled at each station and analyzed for amplitude changes just like in the observed time series.

Most of T1 simulations results (except with the ISAM and JULES ecosystem models) produce a significant increase in $AMP_{P\text{-}T}$ at boreal (north of 50°N) stations (Figure 1a), though there are differences among models. In comparison with the observed average trend (0.094 ± 0.033 ppm yr^{-1}) of $AMP_{P\text{-}T}$ at the 8 boreal stations with a significant increase in $AMP_{P\text{-}T}$, three models show a larger $AMP_{P\text{-}T}$ positive trend (CLM4.5: 0.105 ± 0.046 ppm yr^{-1}; LPJ: 0.101 ± 0.053 ppm yr^{-1}; VISIT: 0.101 ± 0.059 ppm yr^{-1}). At the three boreal stations with no significant trend in observed $AMP_{P\text{-}T}$ (BAL, MHD, SHM in Figure 1a), the T1 simulation results also correctly reproduce no trend (Figure 1a) except for ORCHIDEE at MHD and VISIT at SHM.

Similar to trends in $AMP_{P\text{-}T}$, statistically significant increasing trough-to-peak CO_2 amplitude ($AMP_{T\text{-}P}$) is found in the T1 simulation results (except again for ISAM and JULES), consistent with the observed trends. For the simulations with ISAM and JULES, temperate sites have more statistically significant increasing trends of $AMP_{T\text{-}P}$ than boreal and Arctic sites.

Overall, unlike previous studies that have shown a systematic underestimation of AMP trend by ecosystem models, namely the CMIP5 models (Taylor et al., 2012) and the MsTMIP models (Huntzinger et al., 2013; Wei et al., 2014) at high northern latitudes (Graven et al., 2013; Thomas et al., 2016), we found both underestimation and overestimation of AMP trends from the TRENDYv2 models (Figure S4). This phenomenon can be related to different climate forcing (between CMIP5 and other ensembles), partly different terrestrial ecosystem models, and the transport simulation with a different transport model (LMDZ4 here instead of TM3 and ACTM in Graven et al. (2013) and TM3 in Thomas et al. (2016)).

Effects of different factors on the trend in AMP_{P-T}

In order to separate the contribution of different driving factors on the trend of AMP_{P-T}, we performed transport simulations with Net Ecosystem CO_2 Exchange (NEE) changes caused by different factors from factorial runs of the TRENDYv2 models, respectively with variable CO_2 only (eCO_2), variable CO_2 and climate, and variable CO_2, climate and land cover change (Table S4, see Methods). To further separate the contribution of atmospheric transport trends to AMP trends, the LMDZ4 transport model was used with variable transport fields (Dee et al., 2011) but constant NEE, air-sea CO_2 flux and fossil fuel and cement emissions of the year 1979, so that trends in AMP from this simulation can be attributed to transport trends only.

The impact of climate change on NEE affecting AMP_{P-T} trends estimated from multi-model ensemble mean (MMEM) varies among stations (Figure 2a). We find a positive trend of AMP induced by climate change at boreal atmospheric stations (8 of 11 stations north of 50°N (Figure. 2a and S5b). On average, climate change caused an enhancement of 0.015±0.025 ppm yr^{-1} in AMP_{P-T} over boreal region (north of 50 ^oN) (Figure 3a), which is about 20% of the observed AMP_{P-T} trend. It has been suggested that warmer temperature is associated with higher vegetation productivity of boreal ecosystems in spring through advancing vegetation green-up date (Keeling et al., 1996), although such positive effect may saturate (Piao et al., 2014; Fu et al., 2015). As shown in Figure S6a, for the BRW site (71 ^oN), the effect of climate change on AMP_{P-T} is positive mainly during May and June.

By contrast at the temperate sites (in the band of 23-50 ^oN), the effect of climate change on the AMP_{P-T} trends is mainly negative (10 of the 15 stations), althoguh the impact is not statsitiscallly significant (except TAP significant at $P<0.05$ and ASK marginally significant at $P<0.1$). On average, climate change is modeled to cause a decrease of AMP_{P-T} of -0.012±0.040 ppm yr^{-1} at stations in the temperate band (Figure 3a). Analysis of NEE impacted by climate change (Trendy models S2 – S1 simulations) shows that climate change alone caused a decrease in CO_2 uptake from April to August over western and central US, in Eastern Europe, northeast China and Mongolia (Fig. S7b), associated with declining soil moisture driven by rising temperature and decreasing precipitation in these regions (Sitch et al., 2015).

In the simulations of CO_2 with MMEM, eCO2 causes a statistically significant increase in AMP_{P-T} at 10 of the 11 boreal stations (Figure 2a), and the magnitude of trend in AMP_{P-T} driven by eCO2 (0.036 ± 0.005 ppm yr^{-1}) is about twice as large as that caused by climate change (Figure 3a). This larger effect of eCO2 than climate change on AMP_{P-T} trends in boreal zone is also present in simulations with individual ecosystem model NEE (Figure S5a and b). This result do not support previous findings by the study of Forkel et al. (2016) which suggest a more prominent signal of climate change than eCO2 in the observed increase in AMP_{P-T} in high northern latitudes. However, we agree that climate change rather than eCO2 causes the latitudinal difference of trend in AMP_{P-T}. As shown in Figure 3a, we found that the magnitude of eCO2 effect to increase the trend of AMP in temperate regions (0.028 ± 0.023 ppm yr^{-1}) is comparalbe to that in boreal regions, although less stations (9 of 15) show statistically significant effect (Figure 2a). It should be noted that four TRENDY models (CLM4.5, ISAM, LPX and OCN) considered carbon-nitrogen interactions and nitrogen deposition, thus the signal of eCO_2 derived from these models includes the interactive effect of nitrogen deposition. Another simulation with nitrogen deposition using CLM4 model (Oleson et al., 2010; Mao et al., 2013) (see Methods) predicts that, however, the effect of nitrogen deposition on AMP_{P-T} trend is not significant ($P<0.05$) at all sites (Figure S8a), while this result depends on individual model parameterizations (Galloway *et al.*, 2008). Further studies based on multiple models with C-N interactions are needed.

Both forest inventory data and model simulation show that afforestation and forest regrowth after abandonment of agriculture in northern ecosystems have an important role in the regional and global carbon balance (Pan et al., 2011; Houghton et al., 2015; FAO, 2015). As shown in Figure S7c, most TRENDYv2 DGVMs (except ISAM) predict that land use change enhance net carbon uptake during the period from April to August in Eastern Europe, China and central and eastern United States. Accordingly, a significant ($P<0.05$) or marginally significant ($P<0.10$) positive effect of LUC on the trend in AMP_{P-T} is predicted across 6 boreal sites and 3 northern temperate sites (Figure 2a and S5c), although the magnitude of signal is generally smaller than the effect of eCO_2 and climate change. Overall, the positive increase of AMP_{P-T} attributed to land use change is similar between boreal region (0.007±0.009 ppm yr^{-1}) and northern temperate region (0.004±0.008 ppm yr^{-1}) (Figure 3a), suggesting that the latitudinal difference in observed AMP_{P-T} increase (0.07±0.05 ppm yr^{-1} in boreal zone and 0.01±0.05 ppm yr^{-1} in temperate zone) has little linkage with land use change. It should be noted that, however, there are still large uncertainties in estimating land-use-change effect on AMP_{P-T} trend, primarily owing to processes of land use change and management not considered in some Trendy models (e.g., wood harvest, shifting cultivation, peat fires) (Table S3) and the lack of some critical processes (e.g., human settlement, erosion/redeposition, woody encroachment) in all models (Houghton et al., 2012).

Over the past thirty years, global CO_2 emissions from fossil fuel consumption have increased from 5.3 Pg C yr^{-1} in 1980 to 9.7 Pg C yr^{-1} in 2012 (Boden et al., 2016, Figure S9a). However, the pattern of change is not spatially uniform in northern hemisphere. A substantial significant increase in annual fossil fuel CO_2 emissions is found over northern temperate region, whereas a significant decline is found in boreal region (Figure S9a). This heterogeneity is also found in the period of April to August, during which AMP_{P-T} is calculated for most northern temperate and boreal stations (Figure S9b). As a result, effect of changes in fossil fuel carbon emissions on the trend in AMP_{P-T} is opposite between temperate and boreal sites, although most sites show non-significant trend in AMP_{P-T} caused by trends of fossil CO_2 emissions. As shown in Figure 2a, a negative effect of fossil fuel emissions on AMP_{P-T} trend is simulated at temperate sites (13 of 15 sites show negative trend with 3 significant sites and 1 marginally significant site) (Figue 2a), and a positive effect at most boreal sites (8 of 11 sites). The absolute value of the AMP_{P-T} trend associated with fossil fuel emissions is generally larger at temperate (average of -0.013±0.022 ppm yr^{-1}) compared to boreal sites (average of 0.003±0.007 ppm yr^{-1}) (Figure 3a).

A recent study (Horton et al., 2015) demonstrated robust trends in sub-seasonal atmospheric circulation patterns over mid-latitude regions during 1979-2013, particularly in summer and autumn. Such changes in the large-scale atmospheric circulation may exert an effect on the trend of CO_2 amplitude. As shown in Figure 2a, although only two stations (UUM and IZO) show statistically significant impact of transport trends on the trend of AMP_{P-T}, the magnitude of transport caused AMP_{P-T} trend is comparable or even larger than the effect of climate change and eCO_2 on NEE at some atmospheric stations, particularly in the temperate zone. For example, at UUM, the observed decrease in AMP_{P-T} is primary caused by change in wind (Figure 2a). In terms of effects air-sea fluxes on the trend of AMP_{P-T}, a weak contribution to AMP trends was simulated across most of sites except at BRW (0.010 ppm yr^{-1}, $P<0.05$, 10% of the observed trend) and MBC (0.015 ppm yr^{-1}, $P<0.1$, 16% of the observed trend).

The mechanisms driving the trend in AMP_{P-T} are here analyzed with observations at the Arctic station of BRW (71°N), the longest northern high latitude CO2 record showing an increase of amplitude of 35% since 50 years, larger than at the Mauna Loa longest record located in the sub-tropics (e.g. Graven et al., 2013; Zeng et al., 2014; Gray et al., 2014; Barlow et al., 2015; Forkel *et al.*, 2016). Our transport simulations with multi-model ensemble mean (MMEM) NEE produce that AMP_{P-T} at the BRW site significantly inreased by about 0.095 ppm yr^{-1} from 1980 to 2012, which is comparable with the observed trend of 0.097 ppm yr^{-1} (Figure 1a). eCO_2 is identified as the largest contributor of increasing AMP_{P-T} with a trend of 0.039 ppm yr^{-1} (40% of the observed trend, $P<0.05$), followed by climate change with a trend of 0.031 ppm yr^{-1} (32% of the observed trend, $P<0.05$) (Figure S5a and b). The effect of ocean flux is of 0.010 ppm yr^{-1} (10% of observed trend, $P<0.05$), and land use change has marginally significant contributions (0.003 ppm yr^{-1} and 3% of observed trend, $P<0.1$) (Figure S5c and e). For other factors such as fossil fuel emissions and transport (Figure S5d and f), non-significant impacts on AMP_{P-T} trend were produced.

Effects of different factors on trend in AMP_{T-P}

We also assessed the effect of different factors on trend in AMP_{T-P} with the same NEE and transport model simulation results (See Methods). In contrast to carbon uptake period, climate change accelerates carbon release from boreal ecosystems during the non-carbon uptake period. As shown in Figure 2b, an increasing AMP_{T-P} (a negative trend in AMP_{T-P} indicates a larger release) is simulated at 8 of the 11 boreal sites (1 site significant at $P<0.05$;

2 sites marginally significant at 0.05<P<0.1). In contrast, a decreasing AMP_{T-P} (shown with positive trend) is produced at 12 of 15 temperate sites (1 site significant at P <0.05; 1 site marginally significant at 0.05<P <0.1) (Figure 2b). It has been suggested that autumn warming enhance vegetation productivity through delaying vegetation senescence, as well as accelerate ecosystem respiration (Piao et al., 2008; Vesala et al., 2010). Therefore, the opposite effect of climate change on the trend of AMP_{T-P} in boreal region (-0.016±0.027 ppm yr^{-1}) and temperate region (0.011±0.040 ppm yr^{-1}) (Figure 3b) is probably due to different magnitude of the response of vegetation productivity (GPP) and ecosystem respiration (TER) to climate change. Indeed, the model results show that the rising temperature induced increase of TER is greater than that of GPP in high northern latitudes, whereas the increase of GPP is larger in temperate regions (Figure S10).

Atmospheric CO_2 simulations from MMEM NEE produce an increasing AMP_{T-P} in response to eCO_2 at 25 of 26 temperate and boreal sites (19 sites significant at P<0.05; two sites marginally significant at 0.05<P<0.1, Figure 2b). NEE from 6 out of 8 terrestrial ecosystem models (except ISAM and JULES) also produces an enhancing AMP_{T-P} from eCO2 (Figure S11a). This result indicates an acceleration of carbon release during the non-carbon uptake period as an indirect effect of the NEE response to eCO2. This is due to the increment in carbon storage caused by the enhancement of net carbon uptake during the carbon uptake period under the effect of eCO_2, which stimulates ecosystem respiration during the non-carbon uptake period (Figure S12). Similar to the contribution of land use change to the trends of AMP_{P-T}, we also found statistically significant enlargement of AMP_{T-P} in response to land use change at 9 of 26 sites (Figure 2b).

Similar to the effect on AMP_{P-T}, the contribution of fossil fuel CO_2 emissions, air-sea fluxes and transport on the trend of AMP_{T-P} is only statistically significant at a minority of sites (only 1, 4 and 2 sites significant at P<0.05 for the effect of fossil fuel, air-sea fluxes and transport, respectively) (Figure 2b). However, the magnitude of signal induced by transport and fossil fuel emissions is generally remarkable over temperate region (Figure 3b), causing an average impact of -0.014±0.036 ppm yr^{-1} and 0.010±0.014 ppm yr^{-1} in the trend of AMP_{P-T}, respectively.

Overall, the observed significant enlargement of AMP_{T-P} at the BRW site (-0.090 ppm

yr^{-1}) is mainly driven by eCO2 (-0.038 ppm yr^{-1} and 42% of observing trend, $P<0.05$), climate change (0.032 ppm yr^{-1} and 35% of observing trend, $P<0.05$), ocean flux change (-0.010 ppm yr^{-1} and 11% of observing trend, $P<0.05$) and land use change (-0.003 ppm yr^{-1} and 4% of observing trend, $P<0.05$).

Conclusion

It is difficult to attribute trends in seasonal atmospheric CO_2 concentration both because of regionally different contributions, and because terrestrial ecosystem models lack mechanisms or did not report separately disturbance contributions and nitrogen deposition contributions. Unlike previous studies based on one model only (Zeng et al., 2014; Forkel et al., 2016), our results based on an ensemble of models to capture the amplitude trends suggest that rising atmospheric CO_2 concentration is the primary driver of enhancement of both $AMP_{P\text{-}T}$ and $AMP_{T\text{-}P}$**,** although climate change plays a critical role and contributes largely to the latitudinal difference of AMP trend. In addition, the effect of other factors such as land use change, fossil fuel emissions, ocean flux, and transport on the trend in $AMP_{P\text{-}T}$ and $AMP_{T\text{-}P}$ is not statistically significant at most of stations, but still large enough to cancel out the effect of eCO_2 at some temperate sites where the observing seasonal CO_2 trends are small. However, the large uncertainties in the forcing data on land use change and fossil fuel emission at the moment do not allow an unequivocal statement on the contribution of these factors, and further studies based on spatially and temporally explicit historic data sets including land use and fossil fuel emission are needed. Finally, we found that rising atmospheric CO_2 concentration has opposite implication in the northern ecosystem carbon balance between carbon uptake period (trend of $AMP_{P\text{-}T}$) and non-carbon uptake period (trend of $AMP_{P\text{-}T}$), due to the lagged effects of increase in carbon storage during carbon uptake period on carbon cycle in non-carbon uptake period. Our results not only provide insights for large-scale field experiments, but also highlight the importance of understanding the carbon releasing processes during the non-growing season, which is critical for reliable projection of global carbon cycle, and thus, the future climate change.

Methods

Atmospheric CO_2 concentration data. Weekly atmospheric CO_2 concentration data were obtained from the Earth System Research Laboratory, National Oceanic and Atmospheric Administration (NOAA-ESRL) archive (Masarie et al., 2014) for the period of 1980-2012. 26 northern temperate and boreal stations with observations longer than 15 years (Table S1) are included in our analyses, given the focus of our study is the long-term trend, which would not be robust without long-term observations. The seasonal curves of atmospheric CO_2 at each station were extracted by fitting the observation data with a function consisting of quadratic polynomial for the long-term trend, four-harmonics for the annual cycle, and a 80-days Full-Width Half-Maximum value (FWHM) averaging filter and a 390-days FWHM averaging filter to further remove short term variations and remaining annual cycles still present in the residuals after the function fit (Thoning et al., 1989). The processing process is incorporated in the standard CO_2 data processing software (CCGCRV) developed by NOAA-ESRL (Thoning et al., 1989). From the seasonal curve of atmospheric CO_2, we then obtained the amplitude and monthly concentration difference.

Land-atmosphere CO_2 exchange. An ensemble of eight dynamic global vegetation models (DGVMs) from TRENDYv2 was used to simulate monthly land-atmosphere CO_2 exchange (Net Biome Productivity, NBP) for the period 1979-2012. These models were coordinated to perform three simulations (S1, S2 and S3) following the TRENDYv2 protocol (Le Quéré *et al.*, 2013; Sitch *et al.*, 2015). In simulation S1, only atmospheric CO_2 was varied. In simulation S2, only atmospheric CO_2 and climate were varied. In simulation S3, atmospheric CO_2, climate and land use were varied. The effects of rising atmospheric CO_2, climate change and land use change on NBP can then be obtained from S1, the difference between S2 and S1, and the difference between S3 and S2, respectively. Among the eight TRENDY models, four models (CLM4.5, ISAM, LPX and OCN) considered carbon-nitrogen interactions and nitrogen deposition through simulation S1 to S3. All models used the same forcing datasets, of which global atmospheric CO_2 concentration was from the combination of ice core records and atmospheric observations (Keeling & Whorf, 2005 and update); historical climate fields were from CRU-NCEP dataset (http://dods.extra.cea.fr/data/p529viov/cruncep/); land use data was from the Hyde database (Hurtt et al., 2011). The effect of nitrogen deposition was derived from an additional simulation (S4) performed by CLM4 model

(Oleson *et al.*, 2010; Mao *et al.*, 2013) in which all the driving factors (atmospheric CO_2, climate and land use) were kept constant at 1980 value except transient nitrogen deposition from 1980 through 2012 (Lamarque *et al*., 2005). Detailed information of the nine DGVMs used in this study is listed in Table S2.

Ocean-atmosphere CO_2 exchange. A biogeochemical model PlankTOM5 combined with a global ocean general circulation model NEMO (NEMO-PlankTOM5) were used to simulate the physical, chemical and biological processes that affect the surface ocean CO_2 concentration and thus the ocean-atmosphere CO_2 exchange (Buitenhuis *et al.*, 2010; Le Quéré *et al.*, 2015). The PlankTOM5 model was forced by inputs of ions and compounds from river, sediment and dust (Cotrim da Cunha *et al.*, 2007; Aumont *et al.*, 2003). The NEMO model was driven by daily wind and precipitation from NCEP reanalysis (Kalnay *et al.*, 1996). Further details can be found in Buitenhuis *et al.* (2010).

Fossil fuel CO_2 emission. A gridded monthly time series of fossil fuel CO_2 emissions from CDIAC were constructed based on proportional-proxy approach (Andres et al., 2011; Boden et al., 2016). Firstly, available monthly fossil fuel consumption data from 21 countries was compiled, which account for about 80% of global total emissions. Then these data were used as a proxy for all remaining countries without monthly data based on countries' similarities in climates and economies (for few countries, geographic closeness was also considered). For some years without explicit monthly data, Monte Carlo methods were used to apply data in years with known monthly fractions to those missing-data years. Further details can be found in Andres *et al.* (2011).

The atmospheric transport model. We used LMDZ4, a global tracer transport model (Hourdin et al., 2013) driven by the re-analysis 3-D atmospheric wind fields from the European Centre for Medium-Range Weather Forecasts (Dee et al., 2011), to transform land-atmosphere CO_2 exchange, fossil fuel CO_2 emission and ocean-atmosphere CO_2 exchange into point estimates of CO_2 concentration at 26 sites. The model configuration we used has a horizontal spatial resolution of 3.75° longitude × 2.5° latitude with 19 vertical layers.

To separate the effects of changes in atmospheric CO_2 ('CO_2'), climate ('CLIM'), land use ('LU'), fossil fuel ('FF'), ocean carbon flux ('Ocean') and atmospheric transport ('Wind') on seasonal atmospheric CO_2 concentration change, we designed eight transport simulations (T1~T8, see Table S3). The first one (T1) used time-varying monthly land-atmosphere CO_2 exchange under scenario S3 (driven by rising CO_2, climate change and land use change), fossil fuel CO_2 emission, and ocean-atmosphere CO_2 exchange coupled with LMDZ4 transport model having variable winds, indicating the combined effects of 'CO_2', 'CLIM', 'LU', 'FF', 'Ocean' and 'Wind'. To assess the contribution of 'Wind', the LMDZ4 transport experiment was force by historical varying wind but constant land-atmosphere CO_2 exchange, fossil fuel CO_2 emission and ocean-atmosphere CO_2 exchange in 1979 (T6). Next, to investigate the single effect of 'CO_2', 'CLIM' and 'LU', we utilized LMDZ4 model with varying winds to perform another three transport simulations (T2, T3 and T4, see Table 3) in which fossil fuel CO_2 emission and ocean-atmosphere CO_2 exchange were constant at 1979 value but land-atmosphere CO_2 exchange was varying under three scenarios (S1, driven by CO_2; S2, driven by CO_2 and CLIM; S3, driven by CO_2, CLIM and LU). Consequently, the single effect of 'CO_2' on seasonal CO_2 variation can be assessed by the difference between T2 and T6, that of 'CLIM' from the difference between T3 and T2, and that of 'LU' from the difference between T4 and T3. In addition, we prescribed varying land-atmosphere CO_2 exchange from CLM4 model under scenario S4 (only nitrogen deposition varying), constant fossil fuel CO_2 emission and ocean-atmosphere CO_2 exchange to LMDZ4 model with constant winds (transport simulation T5) to obtain the effect of nitrogen deposition. Finally, to gain the single effect of 'FF' and 'Ocean' on CO_2 seasonal variation, we performed another two simulations in which only fossil fuel CO_2 emission or ocean-atmosphere CO_2 exchange was varying in addition to variable winds (T7 and T8). Thus the contribution of 'FF' can be calculated from the difference between T7 and T6, and that of 'Ocean' from the difference between T8 and T6.

Reference

1. Bacastow, R. B., Keeling, C. D., Whorf, T. P. Seasonal amplitude increase in atmospheric CO_2 concentration at Mauna Loa, Hawaii, 1959–1982. *J. Geophys. Res. D* **90**, 10529-10540 (1985).
2. Kohlmaier, G. H. *et al*. Modelling the seasonal contribution of a CO_2 fertilization effect of the terrestrial vegetation to the amplitude increase in atmospheric CO_2 at Mauna Loa Observatory. *Tellus* **41B**, 487-510 (1989).
3. Keeling, C. D., Chin, J. F. S. & Whorf, T. P. Increased activity of northern vegetation inferred from atmospheric CO_2 measurements. *Nature* **382**, 146–149 (1996).
4. Randerson, J. T., Thompson, M. V., Conway, T. J., Fung, I. Y. & Field, C. B. The contribution of terrestrial sources and sinks to trends in the seasonal cycle of atmospheric carbon dioxide. *Glob. Biogeochem. Cycles* **11**, 535-560 (1997).
5. Piao, S. *et al*. Net carbon dioxide losses of northern ecosystems in response to autumn warming. *Nature* **451**, 49-52 (2008).
6. Graven, H. D. *et al*. Enhanced seasonal exchange of CO_2 by northern ecosystems since 1960. *Science* **341**, 1085-1089 (2013).
7. Zeng, N. *et al*. Agricultural Green Revolution as a driver of increasing atmospheric CO_2 seasonal amplitude. *Nature* **515**, 394-397 (2014).
8. Gray, J. M. *et al*. Direct human influence on atmospheric CO_2 seasonality from increased cropland productivity. *Nature* **515**, 398-401 (2014).
9. Barlow, J. M., Palmer, P. I., Bruhwiler, L. M. & Tans, P. Analysis of CO_2 mole fraction data: first evidence of large-scale changes in CO_2 uptake at high northern latitudes. *Atmos. Chem. Phys.* **15**, 7089-7139 (2015).
10. Forkel, M. *et al*. Enhanced seasonal CO_2 exchange caused by amplified plant productivity in northern ecosystems. *Science* **351**, 696-699 (2016).
11. Foley, J. A. *et al*. Global consequences of land use. *Science* **309**, 570-574 (2005).
12. Piao, S. *et al*. Evaluation of terrestrial carbon cycle models for their response to climate variability and to CO_2 trends. *Glob. Change Biol.* **19**, 2117-2132 (2013).

13. Ciais, P. *et al*. Carbon and Other Biogeochemical Cycles. In: *Climate Change 2013: The Physical Science Basis. Contribution of Working Group I to the Fifth Assessment Report of the Intergovernmental Panel on Climate Change*. Cambridge University Press (2014).
14. Le Quéré, C. *et al.* Global carbon budget 2015. *Earth Syst. Sci. Data* **7**, 349-396 (2015).
15. Chan, D., Ishizawa, M., Higuchi, K., Maksyutov, S. & Chen, J. Seasonal CO_2 rectifier effect and large-scale extratropical atmospheric transport. *J. Geophys. Res.* **113**, doi:10.1029/2007JD009443 (2008).
16. Zhang, X., Gurney, K. R., Rayner, P., Baker, D. & Liu Y. P. Sensitivity of simulated CO_2 concentration to sub-annual variations in fossil fuel CO_2 emissions. *Atmos. Chem. Phys.* **16**, 1907-1918 (2016).
17. Landschützer, P. *et al*. The reinvigoration of the Southern Ocean carbon sink. *Science* **349**, 1221-1224 (2015).
18. Le Quéré, C. *et al.* Global carbon budget 2013. *Earth Syst. Sci. Data* **6**, 235-263 (2014).
19. Sitch, S. *et al*. Recent trends and drivers of regional sources and sinks of carbon dioxide. *Biogeosciences* **12**, 653–679 (2015).
20. Hourdin, F. *et al*. Impact of the LMDZ atmospheric grid configuration on the climate and sensitivity of the IPSL-CM5A coupled model. *Clim. Dynam.* **40**, 2167-2192 (2013).
21. Andres, R. J., Gregg, J. S., Losey, L., Marland, G. and Boden, T. A. Monthly, global emissions of carbon dioxide from fossil fuel consumption. *Tellus* **63B**, 309-327 (2011).
22. Boden, T. A., Marland, G. & Andres, R. J. Global, regional, and national fossil-fuel CO_2 Emissions. Carbon Dioxide Information Analysis Center, Oak Ridge National Laboratory, U.S. Department of Energy, Oak Ridge, Tenn., U.S.A. doi 10.3334/CDIAC/00001_V2016 (2016).
23. Buitenhuis, E. T., Rivkin R. B., Sailley, S. & Le Quéré, C. Biogeochemical fluxes through microzooplankton. *Glob. Biogeochem. Cycles* **24**, GB4015, doi:10.1029/2009GB003601 (2010).
24. Hoeting, J. A., Madigan, D., Raftery A. E. & Volinsky, C. T. Bayesian model averaging: a tutorial. *Statistical Science* **14**, 382-401 (1999).
25. Vrugt, J. A, Diks, C. G. H. & Clark, M. P. Ensemble Bayesian model averaging using Markov Chain Monte Carlo sampling. *Environ. Fluid Mech.* **8**, 579-595 (2008).

26. Zhu, Z. *et al.* Greening of the Earth and its drivers. *Nat. Clim. Change*, *10.1038/nclimate3004 (*2016)

27. Piao, S. *et al*. Evidence for a weaking relationship between interannual temperature variability and northern vegetataion activity. *Nat. Commun.* **5,** doi:10.1038/ncomms6018 (2014).

28. Fu, Y. H. *et al*. Declining global warming effects on the phenology of spring leaf unfolding. *Nature* **526**, 104–107 (2015).

29. Hungate, B. A., Dukes, J. S., Shaw, M. R., Luo, Y. & Field, C. B. Nitrogen and climate change. *Science* **302**, 1512-1513 (2003).

30. Zaehle, S. & Friend, A. D. Carbon and nitrogen cycle dynamics in the O-CN land surface model: 1. Model description, site-scale evaluation, and sensitivity to parameter estimates. *Glob. Biogeochem. Cycles* **24**, doi:10.1029/2009GB003521 (2010).

31. Pan, Y. *et al*. A large and persistent carbon sink in the world's forests. *Science* **333**, 988-993 (2011).

32. Houghton, R. A., Byers, B. & Nassikas, A. A. A role for tropical forests in stabilizing atmospheric CO_2. *Nat. Clim. Change* **5**, 1022-1023 (2015).

33. Lloret, J. & Valiela, I. Unprecedented decrease in deposition of nitrogen oxides over North America: the relative effects of emission controls and prevailing air-mass trajectories. *Biogeochemistry*, doi: 10.1007/s10533-016-0225-5 (2016).

34. Waldner, P. *et al*. Sulphate and nitrogen deposition and trend analyses. Forest Condition in Europe, 2012 Technical Report of ICP Forests. Work Report of the Thünen Institute for World Forestry 2012/1/Ed. Lorenz, M. & Becher, G. (2012).

35. Galloway, J. N. *et al*. Transformation of the nitrogen cycle: recent trends, questions, and potential solutions. *Science* **320**, 889-892 (2008).

36. Vesala, T. *et al*. Autumn temperature and carbon balance of a boreal Scots pine forest in Southern Finland. *Biogeosciences* **7**, 163-176 (2010).

37. Masarie, K., Peters, W., Jacobson, A. & Tans, P. ObsPack: a framework for the preparation, delivery, and attribution of atmospheric greenhouse gas measurements. *Earth Syst. Sci. Data* **6**, 375-384 (2014).

38. Thoning, K. W., Tans, P. P. & Komhyr, W. D. Atmospheric carbon dioxide at Mauna Loa

observatory. 2. Analysis of the NOAA GMCC data, 1974-1985. *J. Geophys. Res.* **94,** 8549-8565 (1989).

39. Oleson, K. *et al*. Technical Description of version 4.5 of the Community Land Model (CLM). NCAR Technical Note NCAR/TN 503+STR; The National Center for Atmospheric Research (NCAR): Boulder, Colorado (2013).
40. Clark, D. B. *et al*. The Joint UK Land Environment Simulator (JULES), model description-Part 2: carbon fluxes and vegetation dynamics. *Geosci. Model Dev.* **4**, 701-722 (2011).
41. Sitch, S. *et al*. Evaluation of ecosystem dynamics, plant geography and terrestrial carbon cycling in the LPJ dynamic global vegetation model. *Glob. Change Biol.* **9**, 161-185 (2003).
42. Stocker, B. D. *et al*. Multiple greenhouse-gas feedbacks from the land biosphere under future climate change scenarios. *Nature Clim. Change* **3**, 666-672 (2013).
43. Krinner, G. *et al*. A dynamic global vegetation model for studies of the coupled atmosphere-biosphere system. *Glob. Biogeochem. Cycles* **19**, 1-33 (2005).
44. Kato, E., Kinoshita, T., Ito, A. & Yamagata, Y. Evaluation of spatially explicit emission scenario of land-use change and biomass burning using a process-based biogeochemical model. *J. Land Use Sci.* **8**, 104-122 (2013).
45. Jain, A. K., Meiyappan, P., Song, Y. & House, J. I. CO_2 emissions from land-use change affected more by nitrogen cycle, than by the choice of land-cover data. *Glob. Change Biol.* **19**, 2893-2906 (2013).
46. Oleson, K. W. *et al*. Technical description of version 4.0 of the Community Land Model (CLM). NCAR Technical Note NCAR/TN 478+STR; The National Center for Atmospheric Research (NCAR): Boulder, Colorado (2010).
47. Mao, J. *et al*. Global latitudinal-asymmetric vegetation growth trends and their driving mechanisms: 1982–2009. *Remote Sens.* **5**, 1484-1497 (2013).
48. Dee, D. P. *et al*. The ERA-Interim reanalysis: configuration and performance of the data assimilation system. *Q. J. R. Meteorol. Soc.* **137**, 553-597 (2011).
49. Keeling, C. D. & Whorf, T. P. Atmospheric CO_2 records from sites in the SIO air sampling network. Trends: a compendium of data on global change, 16-26 (2005).

50. Hurtt, G. C. *et al*. Harmonization of land-use scenarios for the period 1500-2100: 600 years of global gridded annual land-use transitions, wood harvest, and resulting secondary lands. *Climatic change* **109**, 117-161 (2011).

51. Lamarque, J. F. *et al*. Assessing future nitrogen deposition and carbon cycle feedback using a multimodel approach: Analysis of nitrogen deposition. *J. Geophys. Res.* **110**, D19303, doi:10.1029/2005JD005825 (2005).

52. Cotrim da Cunha, L., Buitenhuis, E. T., Le Quéré, C., Giraud, X. and Ludwig, W. Potential impact of changes in river nutrient supply on global ocean biogeochemistry. *Global Biogeochem. Cycles* **21**, GB4007, doi:10.1029/2006GB002718 (2007).

53. Aumont, O., Maier-Reimer, E., Blain, S. and Monfray, P. An ecosystem model of the global ocean including Fe, Si, P colimitations. *Global Biogeochem. Cycles* **17**, 1060, doi:10.1029/2001GB001745 (2003).

54. Kalnay, E. *et al*. The NCEP/NCAR 40-year reanalysis project. *Bull. Am. Meteorol. Soc.* **77**, 437-471 (1996).

55. Thomas, R. *et al*. CO_2 and greening observations indicate increasing light use efficiency in northern terrestrial ecosystems. *Geophys. Res. Lett.* (2016).

56. Horton, D. E. *et al*. Contribution of changes in atmospheric circulation patterns to extreme temperature trends. *Nature* **522**, 465-469 (2015).

57. Taylor, K. E., Stouffer, R. J. & Meehl, G. A. An Overview of CMIP5 and the Experiment Design. *Bull. Am. Meteorol. Soc.* **93**, 485-498 (2012).

58. Huntzinger, D. N. *et al*. The North American Carbon Program Multi-Scale Synthesis and Terrestrial Model Intercomparison Project - Part 1: Overview and experimental design. *Geosci. Model Dev.* **6**, 2121-2133 (2013).

59. Wei, Y. *et al*. The North American Carbon Program Multi-Scale Synthesis and Terrestrial Model Intercomparison Project: Part 2 - Environmental Driver Data. *Geosci. Model Dev.* **7**, 2875-2893 (2014).

Figure 1 Observed and modeled trends in CO_2 seasonal peak-to-trough amplitude (AMP_{P-T}) (a) and trough-to-peak amplitude (AMP_{T-P}) (b). Here we calculated the modeled AMP_{P-T}/ AMP_{T-P} trends based on eight TRENDY models and multi-model ensemble mean (MMEM) under T1 transport simulation (see methods). Shown on the top of the figure are the abbreviated names of 26 atmospheric CO_2 concentration measurement sites in northern temperate and boreal regions. We sort the sites according to their latitudes, from 23°N to 90°N. Each row represents trends for different sites, while each column represents trends derived from observation and model simulations at a certain site. Gray grids show insignificant trends ($P > 0.10$), while colored grids without slashes indicate statistically significant ($P < 0.05$) and those with slashes marginal significant ($P < 0.10$). The number in each grid shows the value of the trend. Site abbreviations are defined in Table S1.

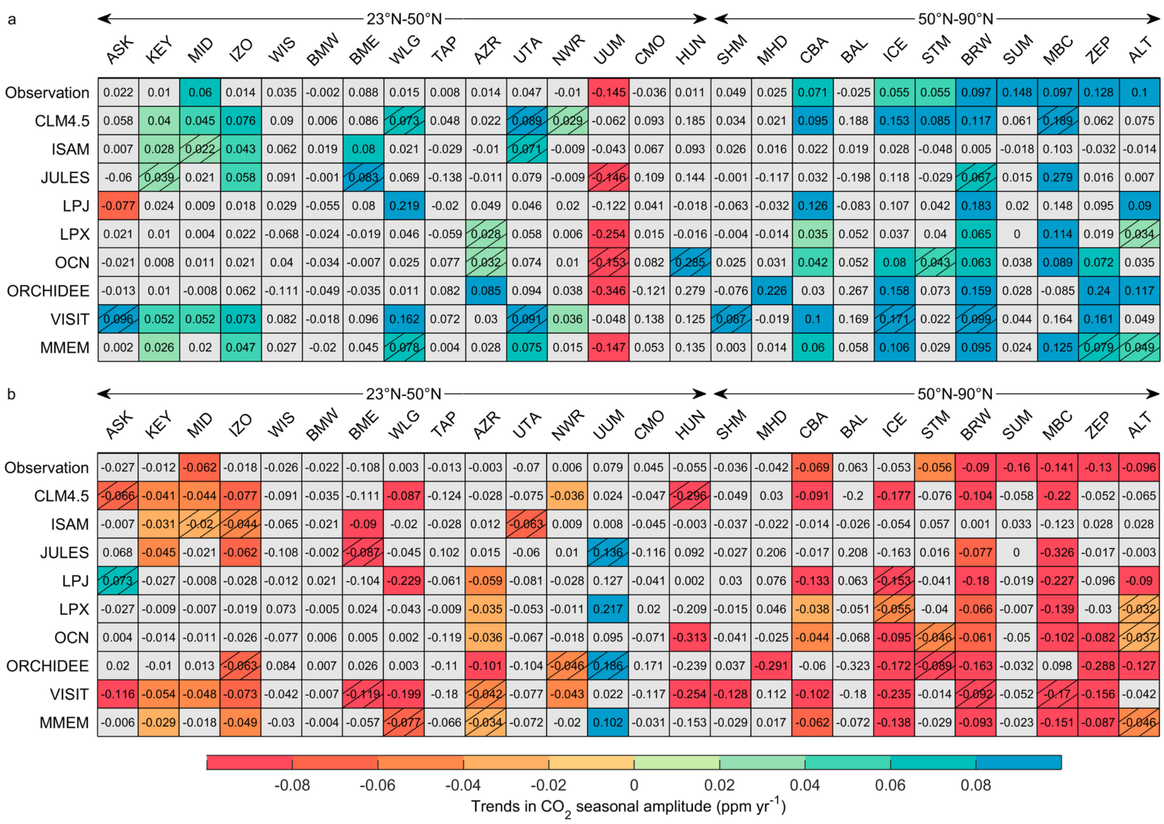

Figure 2 Trends in CO_2 seasonal peak-to-trough amplitude (AMP_{P-T}) (a) and trough-to-peak amplitude (AMP_{T-P}) (b) estimated by multi-model ensemble mean (MMEM) under different scenarios at 26 northern temperate and boreal sites. We present the results according to the latitudinal location of these sites. The single effect of change in atmospheric CO_2 ('CO_2'), climate ('CLIM'), land use ('LU'), fossil fuel ('FF'), ocean-air carbon flux ('Ocean') and wind ('Wind') on CO_2 seasonal amplitudes was derived from transport simulation (T2 - T6), (T3 - T2), (T4 - T3), (T7 - T6), (T8 - T6) and T6, respectively (see Methods and Table S4). For each scenario, we denote those significant (P < 0.05) trends with two dots and marginal significant (P < 0.10) trends with a dot in the middle of the bar.

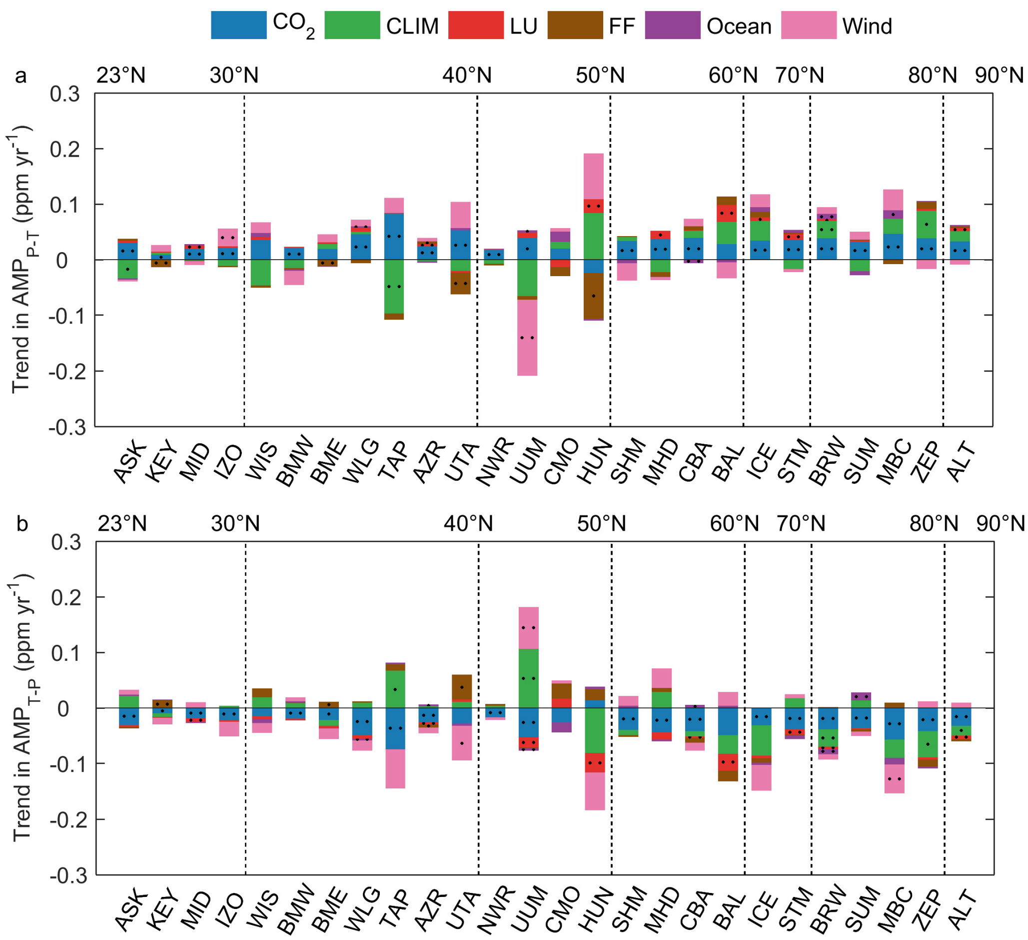

Figure 3 Trends in CO_2 seasonal peak-to-trough amplitude (AMP_{P-T}) (a) and trough-to-peak amplitude (AMP_{T-P}) (b) estimated by multi-model ensemble mean (MMEM) under different scenarios, averaged over northern temperate region (23-50°N) and boreal region (north of 50°N). Model scenario simulations include change in atmospheric CO_2 ('CO_2'), climate ('CLIM'), land use ('LU'), fossil fuel ('FF'), ocean-air carbon flux ('Ocean') and wind ('Wind'). Uncertainties are shown by error bars based on the standard deviation of AMP trends across sites in each region.